Numer Algor
https://doi.org/10.1007/s11075-018-0544-9

ORIGINAL PAPER

Geometric multigrid algorithms for elliptic interface problems using structured grids

Gwanghyun Jo[1] · **Do Y. Kwak**[1]

Received: 29 July 2017 / Accepted: 7 May 2018

Abstract In this work, we develop geometric multigrid algorithms for the immersed finite element methods for elliptic problems with interface (Chou et al. Adv. Comput. Math. **33**, 149–168 2010; Kwak and Lee, Int. J. Pure Appl. Math. **104**, 471–494 2015; Li et al. Numer. Math. **96**, 61–98 2003, 2004; Lin et al. SIAM J. Numer. Anal. **53**, 1121–1144 2015). We need to design the transfer operators between levels carefully, since the residuals of finer grid problems do not satisfy the flux condition once projected onto coarser grids. Hence, we have to modify the projected residuals so that the flux conditions are satisfied. Similarly, the correction has to be modified after prolongation. Two algorithms are suggested: one for finite element spaces having vertex degrees of freedom and the other for edge average degrees of freedom. For the second case, we use the idea of conforming subspace correction used for P_1 nonconforming case (Lee 1993). Numerical experiments show the optimal scalability in terms of number of arithmetic operations, i.e., $\mathcal{O}(N)$ for $\mathcal{V}$-cycle and CG algorithms preconditioned with $\mathcal{V}$-cycle. In $\mathcal{V}$-cycle, we used only one Gauss-Seidel smoothing. The CPU times are also reported.

Keywords Geometric multigrid method · Elliptic interface problem · Finite element method · Interface problem · Structured grid · $\mathcal{V}$-cycle · Optimal scalability

The work of this author is supported by National Research Foundation, contract No. 2017R1D1A1B03032765

✉ Gwanghyun Jo
gwanghyun@kaist.ac.kr

Do Y. Kwak
kdy@kaist.ac.kr

[1] Department of Mathematical Sciences, KAIST, Daejeon, 34341, South Korea

Published online: 07 June 2018

1 Introduction

Multigrid methods are efficient to solve linear systems arising from the discretization of partial differential equations (see [18, 20, 34], for example). The optimal scalability analyses of geometric multigrid methods for elliptic problems are well developed in [4, 6, 7, 20] and references therein. However, geometric multigrid algorithms have the limitation that the algorithms work only on structured grids. On the other hand, there are many PDEs defined on non-rectangular domain or even on the rectangular domain; coefficients may have discontinuity along some smooth interface. For example, the permeability tensor may have jumps across different porous media [17] and dielectric coefficient in Poisson-Boltzmann equations can be discontinuous across the layer between the molecular cell and solvent [33]. To solve such PDEs with finite element methods (FEMs), fitted grids which align the nodes along the material discontinuity are used. Hence, it is hard to implement the geometric multigrid algorithm for the interface problems when the interface has a non-trivial shape.

Recently, immersed finite element methods (IFEMs) which use structured grids were introduced by Li et al. [24, 26, 28, 29] to solve PDEs with interface. We refer to [15, 24, 26, 28, 31] for the convergence analysis of various IFEM schemes. Unlike the conventional FEMs, IFEM allows the interface to cut through the elements. Instead, the basis functions are modified to satisfy the interface conditions along the interface. As noted in [10], one of the biggest advantages of using structured grids is the applicability of multigrid algorithms. A version of algebraic multigrid algorithms was reported in [19], but the performance is not optimal in terms of computational complexity. For example, the number of V-cycles seems to grow as the levels grows, even if they used at least two smoothings on each level. On the other hand, a geometric multigrid algorithm is not reported anywhere, except the Q_1-non-conforming-based IFEM case in [22] where the details are omitted.

In this work, we describe some effective implementations of geometric multigrid algorithm to various IFEMs and report the performance of each algorithm. We consider four different IFEM spaces and we design the multigrid for each of them. Two IFEM spaces are P_1 and Q_1 Lagrangian-based spaces [29, 30] where functions are defined by degrees of freedom (dof). The other IFEM spaces are Crouzeix-Raviart (CR)- and Rannacher-Turek (RT)-based spaces [22, 26] where functions are defined by edge average dof. We first describe the multigrid alrogithms for the Lagrangian-based IFEM space. The difference from the conventional multigrid algorithms is that the prolongation operator $I_k : \widehat{S}_{k-1}(\Omega) \to \widehat{S}_k(\Omega)$ has to be carefully designed so that $I_k u$ satisfies the flux condition, while keeping the nodal values on coarser grids. Other aspects of multigrid algorithms are similar to the standard cases [4, 20, 34]. We see that the performance of multigrid for Lagrangian-based IFEM is optimal in scalability. However, we find that similar multigrid algorithms applied to P_1/Q_1-non-conforming type IFEM are not optimal when the ratio of discontinuity increases. To overcome the difficulty, we project the non-conforming fine grid space (CR/RT) to the corresponding Lagrange-based P1/Q1 IFEMs. Then, we used

the multigrid algorithm developed above. This algorithm is based on the idea of conforming subspace correction, suggested by C. O. Lee [27].

The model problem in this paper is the following second-order elliptic interface problem

$$
\begin{aligned}
-\nabla\cdot\beta\nabla u &= f \quad \text{in} \quad \Omega, && \text{(1a)}\\
[u]_\Gamma &= 0 && \text{(1b)}\\
\left[\beta\frac{\partial u}{\partial \mathbf{n}}\right]_\Gamma &= 0 && \text{(1c)}\\
u &= 0 \quad \text{on} \quad \partial\Omega, && \text{(1d)}
\end{aligned}
$$

where $f \in L^2(\Omega)$, Ω is a convex polygonal domain in $\mathbb{R}^2$, and $\Gamma \subset \Omega$ is a smooth interface which divides the domain into two subdomains Ω^+ and Ω^-. The coefficient β is discontinuous across the interface Γ, where $\beta = \beta^+ \in C^1(\Omega^+)$ and $\beta = \beta^- \in C^1(\Omega^-)$.

We introduce some function spaces and notations. For any bounded domain D, let $H^m(D)$ be the usual Sobolev space of order m with the norm denoted by $\|\cdot\|_{m,D}$. Let us denote a $L^2(\Omega)$ inner product by $(\cdot,\cdot)$. The space $\widetilde{H}^m(D)$ for $m = 1, 2, 3$ is defined as

$$\widetilde{H}^m(D) := \{v \in H^{p(m)}(D) : v|_{D\cap\Omega^s} \in H^m(D\cap\Omega^s), s = +, -\}$$

with the norm

$$\|v\|^2_{\widetilde{H}^m(D)} := \|v\|^2_{H^{p(m)}(D)} + \|v\|^2_{H^m(D\cap\Omega^+)} + \|v\|^2_{H^m(D\cap\Omega^-)}, \quad \forall v \in \widetilde{H}^m(D)$$

where $p(m) = 0$ when $m = 1$ and $p(m) = 1$ when $m = 2, 3$. The set of functions in $\widetilde{H}^2(D)$ which satisfy the homogeneous jump conditions is denoted by

$$\widetilde{H}^2_\Gamma(D) := \{v \in H^1(D) : v \in H^2(D\cap\Omega^s),\ s = +, -,\ \left[\beta\frac{\partial v}{\partial \mathbf{n}}\right]_\Gamma = 0\}.$$

Integration by parts gives the variational problem for the model problem (1): find $u \in H^1_0(\Omega)$ such that

$$\int_\Omega \beta\nabla u\cdot\nabla v\,dx = \int_\Omega f v\,dx \tag{2}$$

for all $v \in H^1_0(\Omega)$. The regularity of solution u for the model problem (1) is well-known [2, 14, 37].

Proposition 1 *Let $f \in L^2(\Omega)$. Then, there exists a unique solution $u \in \widetilde{H}^2(\Omega)$ of problem (2) which satisfies*

$$\|u\|_{\widetilde{H}^2(\Omega)} \le C\|f\|_{0,\Omega}, \tag{3}$$

where C is some positive constant.

The rest of the paper is organized as follows. In Section 2, we review the IFE spaces and review some of the properties. In Section 3, we define our version of

multigrid algorithms. In Section 4, we provide an analysis of the Lagrangian-based multigrid algorithm. The numerical results are given in Section 5 and the conclusion follows in Section 6.

2 Immersed finite element methods

We describe several immersed finite element methods which have been introduced in various papers. First, we define finite element spaces and their norms. Let $\mathcal{T}_h$ be any quasi-uniform triangulations of the domain Ω by triangles or rectangles which do not necessarily align the interface, where h is the maximal diameter of elements. If the interface cuts through some element, we call such an element an interface element. The set of all interface elements in $\mathcal{T}_h$ is denoted by $\mathcal{T}_h^*$. The rest of the elements in $\mathcal{T}_h \setminus \mathcal{T}_h^*$ are non-interface elements. We assume that the mesh size h is sufficiently small so that the interface intersects the edge of an element at no more than two points. If the interface passes through two vertices of an element, then we consider the element is a non-interface element. Let Γ_h be a piecewise linear approximation of Γ, obtained by connecting the points of intersection between Γ and $T \in \mathcal{T}_h^*$. The inner product and norm on an interface element $T \in \mathcal{T}_h^{\gamma,*}$ is understood as piecewise sums

$$(u, v)_{m,T} = (u, v)_{m,T^+} + (u, v)_{m,T^-}, \quad \|\cdot\|_{m,T}^2 = \|\cdot\|_{m,T^+}^2 + \|\cdot\|_{m,T^-}^2$$

for $m = 0, 1$.

2.1 Four immersed finite element spaces

We consider two kinds of IFEM spaces. First kind is Lagrangian-based IFEM spaces: P_1-conforming-based IFE space [29] and Q_1-conforming-based IFEM space [30]. Second is edge average-based IFEM spaces: P_1-non-conforming Crouzeix-Raviart-based IFEM space [26] and Q_1-non-conforming Rannacher-Turek-based IFEM space [22].

We define local spaces on T:

- $S_h^P(T)$ is the space of P_1 functions defined by vertex dof (Lagrange type)
- $S_h^Q(T)$ is the space of Q_1 functions defined by vertex dof (Lagrange type)
- $N_h^P(T)$ is a P_1 non-conforming function [16] defined by edge average dof
- $N_h^Q(T)$ is a Q_1 non-conforming function [36] defined by edge average dof

Lagrangian-based IFEM spaces First, assume T is a triangle element. For a non-interface element $T \in \mathcal{T}_h$, we use standard linear Lagrange nodal base finite element spaces $S_h^P(T)$. For an interface element $T \in \mathcal{T}_h^*$ (see Fig. 1), we modify basis functions ϕ in $S_h^P(T)$ so that the new functions $\widehat{\phi}$ are piecewise linear functions on T:

$$\widehat{\phi} = \begin{cases} \phi^+ = a^+ + b^+x + c^+y, \ (x, y) \in T^+, \\ \phi^- = a^- + b^-x + c^-y, \ (x, y) \in T^-, \end{cases} \tag{4}$$

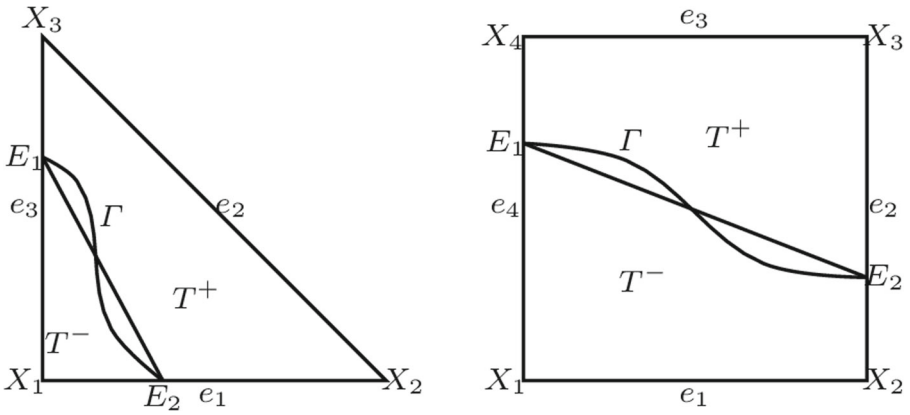

Fig. 1 An interface element for triangle case (left) and rectangle case (right)

The coefficients in (4) are determined by nodal values and interface conditions (1b) and (1c) as follows:

$$\phi(X_i) = G_i, \quad i = 1, 2, 3 \tag{5a}$$

$$\phi^+(E_i) = \phi^-(E_i), \quad i = 1, 2, \tag{5b}$$

$$\int_{\overline{E_1E_2}} \beta^+ \nabla\phi^+ \cdot \mathbf{n}_{\Gamma_h} = \int_{\overline{E_1E_2}} \beta^- \nabla\phi^- \cdot \mathbf{n}_{\Gamma_h}, \tag{5c}$$

where $G_i, i = 1, 2, 3$ are nodal values. The space of such modified basis functions $\widehat{\phi}$ is denoted by $\widehat{S}_h^P(T)$.

For rectangle elements, a similar process defines $\phi \in \widehat{S}_h^Q(T)$ where

$$\widehat{\phi} = \begin{cases} \phi^+ = a^+ + b^+x + c^+y + d^+xy, & (x, y) \in T^+, \\ \phi^- = a^- + b^-x + c^-y + d^-xy, & (x, y) \in T^-, \end{cases}$$

is determined by (5a), (5b), and (5c) and an extra condition that $d^- = d^+$ (see [21, 28]). The global immersed finite element space $\widehat{S}_h^\gamma(\Omega)$ ($\gamma = P$ or Q) is defined as follows:

$$\begin{cases} \phi|_T \in S_h^\gamma(T) & \text{if } T \text{ is a non-interface element,} \\ \phi|_T \in \widehat{S}_h^\gamma(T) & \text{if } T \text{ is an interface element,} \\ \phi|_{T_1}(X) = \phi|_{T_2}(X) & \text{if } T_1 \text{ and } T_2 \text{ are adjacent elements} \\ & \text{and } X \text{ is a common node of } T_1 \text{ and } T_2, \\ \phi(X) = 0 & \text{if } X \text{ is a node on the boundary edges.} \end{cases}$$

Edge average-based IFEM spaces As before, we first consider the triangle element. We modify basis functions ϕ in $N_h^P(T)$ for an interface element $T \in \mathcal{T}_h^*$ so that new functions $\widehat{\phi}$ in (4) are determined by conditions similar to (5a)–(5c) where (5a) is replaced by edge average dof [15],

$$\int_{e_i} \phi = G_i, \quad i = 1, 2, 3. \tag{6}$$

For rectangle elements, a similar process defines $\widehat{\phi} \in \widehat{N}_h^Q(T)$ where

$$\widehat{\phi} = \begin{cases} \phi^+ = a^+ + b^+x + c^+y + d^+(x^2 - y^2), & (x, y) \in T^+, \\ \phi^- = a^- + b^-x + c^-y + d^-(x^2 - y^2), & (x, y) \in T^-, \end{cases}$$

is determined by (6), (5b) and (5c), and an extra condition that $d^- = d^+$ [22].

The global immersed finite element space $\widehat{N}_h^\gamma(\Omega)$ ($\gamma = P$ or Q) is defined as follows:

$$\begin{cases} \phi|_T \in N_h^\gamma(T) & \text{if } T \text{ is a non-interface element,} \\ \phi|_T \in \widehat{N}_h^\gamma(T) & \text{if } T \text{ is an interface element,} \\ \int_e \phi|_{T_1} = \int_e \phi|_{T_2} & \text{if } T_1 \text{ and } T_2 \text{ are adjacent elements} \\ & \text{and } e \text{ is a common edge of } T_1 \text{ and } T_2, \\ \int_e \phi ds = 0 & \text{if } e \text{ is part of the boundary } \partial\Omega. \end{cases}$$

It suffices to consider the cases $\widehat{S}_h(\Omega) = \widehat{S}_h^P(\Omega)$ and $\widehat{N}_h(\Omega) = \widehat{N}_h^P(\Omega)$. The case of $\widehat{S}_h^Q(\Omega)$ or $\widehat{N}_h^Q(\Omega)$ is almost the same.

Interpolation property We remark interpolation properties of IFEM spaces. Let $\pi_h : \widetilde{H}_\Gamma^2(T) \to \widehat{S}_h(\Omega)$ (respectively, $\widehat{N}_h(\Omega)$) be the interpolation operator defined by

$$(\pi_h u)(X_i) = u(X_i) \left(\text{respectively } \int_{e_i}(\pi_h u) = \int_{e_i} u\right), \quad i = 1, 2, 3.$$

The operator π_h is extended to $u \in \widetilde{H}_\Gamma^2(\Omega)$ by $(\pi_h u)|_T = \pi_h(u|_T)$ for each element T. Then, the operator π_h satisfies the following approximation property [21, 26, 28].

Proposition 2 *There exists a constant $C > 0$ such that*

$$\sum_{T \in \mathcal{T}_h} (\|u - \pi_h u\|_{0,T} + h\|u - \pi_h u\|_{1,T}) \le Ch^2 \|u\|_{\widetilde{H}^2(\Omega)}. \tag{7}$$

2.2 Two IFEM methods

Modified Lagrangian-based IFEM There are two versions of IFEM using Lagrange nodal basis element functions [15, 24, 28, 29, 31]. The first kind of IFEM [15, 28, 29] uses a naive variational form. Another kind of formulation [24, 31] was introduced recently to compensate the consistency error by adding the interior penalty terms. It turns out, the second version exhibits optimal order while the first one does not [31, 32].

Now, we describe the IFEM having the interior penalty terms. Let $\mathcal{E}_h$ be a set of all edges of $\mathcal{T}_h$ and let $H_h(\Omega)$ be the space defined by sum of $H_0^1(\Omega)$ and $\widehat{S}_h(\Omega)$, equipped with the norm $\|u\|_{1,h}^2 := \sum_{T \in \mathcal{T}_h} \|u\|_{1,T}^2$. For an interior edge $e \in \mathcal{E}_h$, we associate with a unit normal vector $\mathbf{n}_e$ at e whose direction we fix once and for all. Let $\{v\}_e$ and $[v]_e$ denote the average and jump for $v \in H_h(\Omega)$ on an edge $e \in \mathcal{E}_h$, i.e.,

$$\begin{aligned} \{v\}_e(x) &:= \frac{1}{2} \lim_{\delta \to 0+} (v(x - \delta \mathbf{n}_e) + v(x + \delta \mathbf{n}_e)), \\ [v]_e(x) &:= \lim_{\delta \to 0+} (v(x - \delta \mathbf{n}_e) - v(x + \delta \mathbf{n}_e)). \end{aligned}$$

Multiplying both sides of the (1) by $v \in H_h(\Omega)$ and applying Green's theorem, we have

$$\sum_{T\in\mathcal{T}_h}\int_T \beta\nabla u\cdot\nabla v\,dx-\sum_{e\in\mathcal{E}_h}\int_e\{\beta\nabla u\cdot\mathbf{n}_e\}_e[v]_e\,ds=\int_\Omega f v\,dx. \tag{8}$$

Since the solution u satisfies $[u]_e = 0$ for every edge $e \in \mathcal{E}_h$, we can rewrite (8) as

$$\begin{aligned}&\sum_{T\in\mathcal{T}_h}\int_T \beta\nabla u\cdot\nabla v\,dx-\sum_{e\in\mathcal{E}_h}\int_e\{\beta\nabla u\cdot\mathbf{n}_e\}_e[v]_e\,ds\\&-\sum_{e\in\mathcal{E}_h}\int_e\{\beta\nabla v\cdot\mathbf{n}_e\}_e[u]_e\,ds+\sum_{e\in\mathcal{E}_h}\int_e\frac{\sigma}{h}[u]_e[v]_e\,ds=\int_\Omega f v\,dx.\end{aligned}$$

Here, $\sigma > 0$ is some parameter chosen so that $a_h(\cdot,\cdot)$ becomes coercive on the finite element space $\widehat{S}_h(\Omega)$ (see [24, 31]). Let us define a bilinear form $a_h(\cdot,\cdot) : H_h(\Omega)\times H_h(\Omega)\to\mathbb{R}$ by

$$\begin{aligned}a_h(u,v)=&\sum_{T\in\mathcal{T}_h}\int_T \beta\nabla u\cdot\nabla v\,dx-\sum_{e\in\mathcal{E}_h}\int_e\{\beta\nabla u\cdot\mathbf{n}_e\}_e[v]_e\,ds\\&-\sum_{e\in\mathcal{E}_h}\int_e\{\beta\nabla v\cdot\mathbf{n}_e\}_e[u]_e\,ds+\sum_{e\in\mathcal{E}_h}\int_e\frac{\sigma}{h}[u]_e[v]_e\,ds.\end{aligned} \tag{9}$$

The form in (9) is motivated by Nitsche's consistent scheme [35] and weak forms of discontinuous Galerkin [1].

Then, the IFEM for the problem (1) is to find the solution $u_h \in \widehat{S}_h(\Omega)$ such that

$$a_h(u_h,v)=(f,v)_h,\quad \forall v\in\widehat{S}_h(\Omega), \tag{10}$$

where the inner product $(\cdot,\cdot)_h$ is the usual L^2 inner product. We define the operator $A_h : u_h \in \widehat{S}_h(\Omega)\to\widehat{S}_h(\Omega)$ such that

$$a_h(u_h,v)=(A_h u_h,v)_h.$$

The optimal order of convergence for the solution of this IFEM is given in [31].

Proposition 3 *Let u and u_h be solutions of (1) and (10), respectively. Then, there exists a constant $C > 0$ independent of u and h such that*

$$\|u-u_h\|_{0,\Omega}+h\|u-u_h\|_{1,h}\le Ch^2\|u\|_{\widetilde{H}^3(\Omega)}. \tag{11}$$

Edge average degree of freedom-based IFEM The IFEM space based on the average dof for triangle (or rectangle) grids were introduced in [22, 26]: Find $u_h \in \widehat{N}_h(\Omega)$ such that

$$\sum_{T\in\mathcal{T}_h}\int_T \beta\nabla u\cdot\nabla\phi=(f,\phi)_h,\quad \forall\phi\in\widehat{N}_h(\Omega). \tag{12}$$

Here, we denote the matrix arising system from (12) by A_h^n. The optimal order of convergence for the solution of this IFEM is given in [26].

Proposition 4 *Let u and u_h be solutions of (1) and (12), respectively. Then, there exists a constant $C > 0$ independent of u and h such that*

$$\|u - u_h\|_{0,\Omega} + h\|u - u_h\|_{1,h} \leq Ch^2\|u\|_{\widetilde{H}^2(\Omega)}.$$

3 Multigrid method for IFEM

In this section, we describe multigrid algorithms for two kinds of IFEM described in Section 2.2. Let $\mathcal{T}_{h_k}$, $k = 0, ..., J$ be hierarchical triangulations of Ω with mesh size $h_k = 2^{-k}h_0$, for some positive constant h_0. The collection of nodes for triangulation $\mathcal{T}_{h_k}$ is denoted by V_{h_k}. An element in $\mathcal{T}_{h_k}$ is constructed by connecting the midpoints of the edges of the triangles in $\mathcal{T}_{h_{k-1}}$. For simplicity, we replace the subscript h_k simply by the subscript k when there is no worry of confusion. For example,

$$\mathcal{T}_k = \mathcal{T}_{h_k},\ a_k(\cdot,\cdot) = a_{h_k}(\cdot,\cdot),\ \widehat{S}_k(\Omega) = \widehat{S}_{h_k}(\Omega),\ \widehat{N}_k(\Omega) = \widehat{N}_{h_k}(\Omega),\ (\cdot,\cdot)_k = (\cdot,\cdot)_{h_k}.$$

Firstly, we describe a multigrid algorithm for Lagrangian-based IFEM spaces. For CR and RT types, we describe a multigrid algorithm using Lagrangian-type IFEM subspace correction [22, 27].

3.1 Multigrid algorithm for Lagrangian-based IFEM spaces

To define multigrid algorithms we need a prolongation operator $\widehat{I}_k : \widehat{S}_{k-1}(\Omega) \to \widehat{S}_k(\Omega)$, which is non-trivial when subspaces are not nested. If $v \in \widehat{S}_{k-1}(\Omega)$, then $\widehat{I}_k v \in \widehat{S}_k(\Omega)$ is defined by

$$\widehat{I}_k v(X) = \begin{cases} v(X) & \text{if } X \in V_{k-1}, \\ \frac{1}{2}\left(v(X)|_{T_1} + v(X)|_{T_2}\right) & \text{if } X \text{ is a midpoint of an edge } e \text{ shared} \\ & \text{by two triangles} T_1,\ T_2 \in \mathcal{T}_{k-1}. \end{cases}$$

The operator $\widehat{I}_k$ on a non-interface element T_{k-1} is the same as usual prolongation for conforming FEM [20]. Now, we explain the prolongation of $v \in \widehat{S}_{k-1}(\Omega)$ for interface elements in detail. Referring to the left of Fig. 2, we consider two adjacent elements T_1^{k-1} and T_2^{k-1} in $\mathcal{T}_{k-1}^*$. Note that the union of T_1^{k-1} and T_2^{k-1} is divided by two regions Ω^+ and Ω^-. Assume that the node X_3 belongs to Ω^- and the nodes X_1, X_2, and X_4 belong to Ω^+. Given a function $v \in \widehat{S}_{k-1}(\Omega)$, let $v_i = v|_{T_i^{k-1}}$, $i = 1, 2$. Now consider the mid points of vertices $X_5, X_6, \ldots, X_9$ in the right of Fig. 2. It suffices to consider a typical point, say X_5. Since the node X_5 belongs to Ω^-, $\widehat{I}_k v(X_5)$ is defined as the average values:

$$\widehat{I}_k v(X_5) = \frac{1}{2}\left(v_1^-(X_5) + v_2^-(X_5)\right),$$

where $v_1^- = v_1|_{T_1^{k-1,-}}$ and $v_2^- = v_2|_{T_2^{k-1,-}}$.

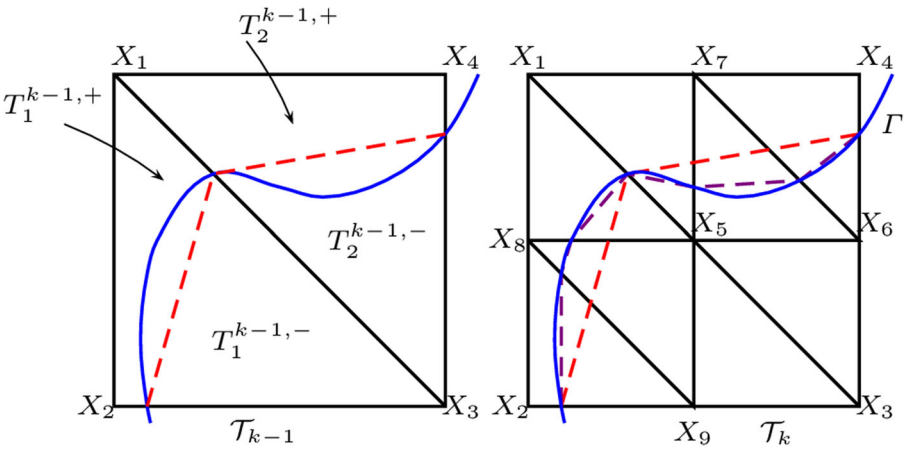

Fig. 2 Interface triangles in $\mathcal{T}_{k-1}$ and $\mathcal{T}_k$. The blue curve represents the interface Γ. The dashed lines represent the approximated interfaces Γ_{k-1} and Γ_k

The restriction operator P_{k-1}^0 is defined as the adjoint operators of $\widehat{I}_k$ with respect to $(\cdot,\cdot)_k$, i.e., for $u \in \widehat{S}_k(\Omega)$ and $\phi \in \widehat{S}_{k-1}(\Omega)$,

$$(P_{k-1}^0 u, \phi)_{k-1} = (u, \widehat{I}_k \phi)_k.$$

Now, we describe multigrid operator $\mathbf{LMG}_k$ from $\widehat{S}_k(\Omega)$ to $\widehat{S}_k(\Omega)$, $(k = 1, 2, \ldots, J)$. Let

$$A_J x = g_J \tag{13}$$

be the linear system obtained from (10) where $g_J \in \widehat{S}_J(\Omega)$. Suppose R_k is a smoothing operator such as Gauss-Seidel or Jacobi and let R_k^t be its adjoint.

Algorithm 1 $\mathbf{LMG}_k$

Set $\mathbf{LMG}_0 g_0 = A_0^{-1} g_0$. Suppose $\mathbf{LMG}_{k-1}$ is defined. We define $\mathbf{LMG}_k g_k$ for $g_k \in \widehat{S}_k(\Omega)$ in recursive way.

1. Set $x^0 = 0$ and $z^0 = 0$
2. Define x^i for $i = 1, ..., m$ by
$$x^i = x^{i-1} + R_k(g_k - A_k x^{i-1})$$
3. Define y^m by $y^m = x^m + \widehat{I}_k z^p$ where z^j for $j = 1, ..., p$ is defined by
$$z^j = z^{j-1} + \mathbf{LMG}_{k-1}[P_{k-1}^0(g_k - A_k x^m) - A_{k-1} z^{j-1}]$$
4. Define y^i for $i = m+1, ..., 2m$ by
$$y^i = y^{i-1} + R_k^t(g_k - A_k y^{i-1})$$
5. Set $\mathbf{LMG}_k g_k = y^{2m}$.

Note that the $\mathbf{LMG}_k$ is a symmetric operator. The cases of $p = 1$ and $p = 2$ correspond to $\mathcal{V}$ and $\mathcal{W}$ cycle, respectively. In particular, when $p = 1$, we will use notation $\mathcal{V}(m, m)$ for the algorithm, i.e., $u = \mathcal{V}(m, m) g_J$.

3.2 Multigrid algorithm for edge average dof-based IFEM spaces

Now, we describe the multigrid algorithms for edge average-based IFEM spaces. The multigrid algorithms using P_1/Q_1-non-conforming space for non-interface problems are considered in [8, 11–13]. The difference between these and from Lagrange type is to use the edge average dof. It is well known that the performance of multigrid for CR and RT is not as good as the case of Lagrange. Still, the behavior is acceptable (see [11–13]). However, for the interface problem, the situation is worse: we found through extensive numerical experiments that the convergence is too slow to use when the ratio β^+/β^- becomes large (or small). This is because the discontinuity of basis in $\widehat{N}_k(\Omega)$ across the edges tends to be large as the jump of β increases. Hence, the necessity for an efficient and robust algorithms has emerged. It turns out that the idea of subspace correction by Lagrangian-type FEM introduced by C. Lee [27] works well for the interface problem, which we describe briefly below.

As is usual with multigrid algorithm, we apply a few presmoothings on the fine space $\widehat{N}_J(\Omega)$. Then, the residuals are transferred to Lagrangian-type IFEM $\widehat{S}_J(\Omega)$. Next, **LMG** is applied on $\widehat{S}_J(\Omega)$. Finally, the result is added to $\widehat{N}_J(\Omega)$ for update followed by postsmoothings. Figure 3 shows one cycle of subspace correction multigrid algorithm.

For this purpose, we need to define the transfer operators between $\widehat{S}_J(\Omega)$ and $\widehat{N}_J(\Omega)$. Let $\mathcal{Q}_c^n$ and $\mathcal{Q}_n^c$ stand for the transfer operators between them. Firstly, $\mathcal{Q}_c^n : u_c \in \widehat{S}_J(\Omega) \to \widehat{N}_J(\Omega)$ is defined in such a way that $\mathcal{Q}_c^n u_c$ has the same edge average with u_c on every element, i.e.,

$$\int_e \mathcal{Q}_c^n u_c = \int_e u_c, \tag{14}$$

for all edges e. For real implementation of (14), we compute

$$\int_e \mathcal{Q}_c^n u_c = \frac{1}{2}\left(\int_e u_c|_{T_1} + \int_e u_c|_{T_2}\right),$$

where $e \in \partial T_1 \cap \partial T_2$.

On the other hand, $\mathcal{Q}_n^c$ is defined as the transpose of $\mathcal{Q}_c^n$, i.e.,

$$(\mathcal{Q}_n^c u_n, u_c)_k = (u_n, \mathcal{Q}_c^n u_c)_k.$$

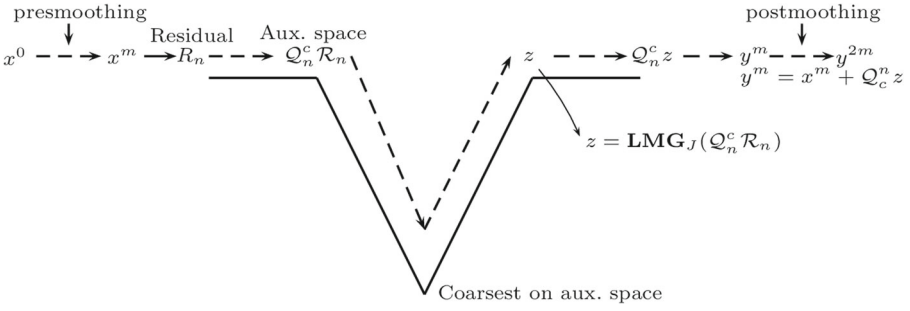

Fig. 3 Non-conforming-conforming $\mathcal{V}$-cycle

Since $\mathcal{Q}_c^n u_c$ in the (14) is computed elementwise, it is very cheap to compute.

We show the computation of $\mathcal{Q}_c^n u_c$ on typical interface element T with three nodes $X_1(0,0)$, $X_2(1,0)$, and $X_3(0,1)$ where the interface cuts through edges at $E_1(0,b)$, $B_2(a,0)$ (see the left of Fig. 1). Let $\widehat{\phi}_j$ $(j=1,2,3)$ be basis functions of $\widehat{S}_h(T)$ associated with X_i, i.e., $\widehat{\phi}_j(X_i)=\delta_{ij}$. Then, $\widehat{\phi}_j$ $(j=1,2,3)$ have the following form

$$\widehat{\phi}_1=\begin{cases} l_1+c_{12}l_2+c_{13}l_3, & \text{in } T^-,\\ c_{11}l_1, & \text{in } T^+,\end{cases}\quad \widehat{\phi}_2=\begin{cases} c_{22}l_2+c_{23}l_3, & \text{in } T^-,\\ c_{21}l_1+l_2, & \text{in } T^+,\end{cases}$$
$$\widehat{\phi}_3=\begin{cases} c_{32}l_2+c_{33}l_3, & \text{in } T^-,\\ c_{31}l_1+l_3, & \text{in } T^+,\end{cases} \tag{15}$$

where l_1, l_2, and l_3 are linear Lagrange nodal basis functions associated with the vertices X_j $(j=1,2,3)$, i.e., $l_j(X_i)=\delta_{ij}$. The coefficients c_{ij} in (15) are explicitly described in [10]. Let $\widehat{\psi}_j$ $(j=1,2,3)$ be basis functions of $\widehat{N}_h(T)$ associated with e_i, i.e., $\frac{1}{|e|}\int_{e_i}\widehat{\psi}_j=\delta_{ij}$. Suppose $\widehat{\phi}=t_1\widehat{\phi}_1+t_2\widehat{\phi}_2+t_3\widehat{\phi}_3$, then $\mathcal{Q}_c^n\widehat{\phi}=r_1\widehat{\psi}_1+r_2\widehat{\psi}_2+r_3\widehat{\psi}_3$, where the relation of coefficients t_i and r_i are given as follows:

$$\begin{bmatrix} r_1\\ r_2\\ r_3\end{bmatrix}=\begin{bmatrix} q_{11} & q_{12} & q_{13}\\ q_{21} & q_{22} & q_{23}\\ q_{31} & q_{32} & q_{33}\end{bmatrix}\begin{bmatrix} t_1\\ t_2\\ t_3\end{bmatrix}.$$

We note that $q_{ij}=\frac{1}{|e_i|}\int_{e_i}\widehat{\phi}_j$. For example,

$$\begin{aligned} q_{11}&=\int_{e_1}\widehat{\phi}_1 dx=\int_0^a (1-x)+xc_{12}\mathrm{d}x+\int_a^1 c_{11}(1-x)\mathrm{d}x\\ &=a-\frac{a^2}{2}+\frac{a^2c_{12}}{2}+\left(\frac{1}{2}-a+\frac{a^2}{2}\right)c_{11}.\end{aligned}$$

We summarize the algorithm to solve

$$A_J^n x=g_J^n,$$

where $g_J^n\in\widehat{N}_J(\Omega)$.

Algorithm 2 NcMG

1. Set $x^0=0$ and $z^0=0$
2. Define x^i for $i=1,...,m$ by
$$x^i=x^{i-1}+R_k(g_J^n-A_J^n x^{i-1})$$
3. Define y^m by $y^m=x^m+\mathcal{Q}_c^n z$ where $z=\mathbf{LMG}_J\mathcal{Q}_n^c(g_J^n-A_J^n x^m)$
4. Define y^i for $i=m+1,...,2m$ by
$$y^i=y^{i-1}+R_k^t(g_J^n-A_J^n y^{i-1})$$
5. Set $\mathbf{NcMG}g_J^n=y^{2m}$.

Note that the **NcMG** is a symmetric operator. We used $\mathcal{V}(m_c,m_c)$ as the inner multigrid cycle $\mathbf{LMG}_J$. For this case, we use notation $\mathcal{N}_m(m_c,m_c)$.

4 Convergence analysis of LMG

In this section, we give analysis for **LMG** for space $\widehat{S}_k^P$. The analyses for the rectangular case ($\widehat{S}_k^Q$) are similar. A main difficulty in the analysis of the multigrid algorithm for the IFEM is that the underlying spaces are not nested, i.e., $\widehat{S}_0(\Omega) \nsubseteq \widehat{S}_1(\Omega) \nsubseteq \ldots \nsubseteq \widehat{S}_J(\Omega)$ because of the interface. We will follow the framework provided in [7], where the convergence of multigrid algorithm for non-nested spaces is given. We first state some assumptions.

(A.1) **Smoothing property**. There exists a constant $C_R > 0$ such that for all $u \in \widehat{S}_k(\Omega)$,

$$\frac{\|u\|_k^2}{\lambda_k} \leq C_R(\tilde{R}_k u, u)_k,$$

where $\tilde{R}_k = (I - K_k^* K_k) A_k^{-1}$, $K_k = I - R_k A_k$ and $K_k^* = I - R_k^t A_k$.

(A.2) There exists a constant C^*, such that

$$A_k(\widehat{I}_k u, \widehat{I}_k u) \leq C^* A_{k-1}(u, u), \quad \forall u \in \widehat{S}_{k-1}(\Omega).$$

(A.3) **Regularity and approximation** For some $0 < \alpha \leq 1$, there exists a constant $C_\alpha > 0$ such that

$$|a_k((I - \widehat{I}_k P_{k-1})u, u)| \leq C_\alpha \left(\frac{\|A_k u\|_k^2}{\lambda_k} \right)^\alpha a_k(u, u)^{1-\alpha}.$$

for all $u \in \widehat{S}_k(\Omega)$.

Then, by the framework in [7], we can conclude the following result.

Theorem 1 *Suppose $p = 2$ and $m(k) = m$ for all k in the algorithm. Assume (A.1), (A.2), and (A.3) hold. If "m is sufficiently large," then we have*

$$|a_k((I - LMG_k A_k)u, u)| \leq \delta a_k(u, u) \quad \forall u \in \widehat{S}_k(\Omega),$$

where

$$\delta = \frac{M}{M + m^\alpha}.$$

We now examine the assumptions (A.1)–(A.3). It is clear that A_k is symmetric positive definite and sparse matrix. For example, each row of A_k has less than 13 non-zero entries if uniform grids are used on rectangular domain. Therefore, standard smoothing operators such as Gauss-Seidel (GS) and Jacobi satisfy (see [5]). Therefore, it suffices to verify (A.2) and (A.3).

We introduce an energy-like norm for the analysis, $|||u_k|||_k = \sqrt{A_k(u_k, u_k)}$. We define $P_{k-1} : \widehat{S}_k(\Omega) \to \widehat{S}_{k-1}(\Omega)$ as adjoint operator of $\widehat{I}_k$, i.e., P_{k-1} satisfies

$$a_{k-1}(P_{k-1}u, v) = a_k(u, \widehat{I}_k v),$$

for all $u \in \widehat{S}_k(\Omega)$ and $v \in \widehat{S}_{k-1}(\Omega)$. We need the following approximation property of the prolongation $\widehat{I}_k : \widehat{S}_{k-1}(\Omega) \to \widehat{S}_k(\Omega)$, which we verify numerically (see Table 1).

Table 1 $\|\widehat{I}_k\pi_{k-1}w - w\|_{1,h_k}$ and $\|P_{k-1}\pi_k w - w\|_{1,h_k}$ for problem (25)

k	$\|\widehat{I}_k\pi_{k-1}w - w\|_{1,h_k}$	order	$\|P_{k-1}\pi_k w - w\|_{1,h_k}$	order
2	2.828E0		5.468E0	
3	1.510E0	0.905	1.510E0	1.856
4	7.538E-1	1.002	8.223E-1	0.877
5	3.855E-1	0.968	3.857E-1	1.093
6	1.931E-1	0.997	1.930E-1	0.999
7	9.675E-2	0.997	9.690E-2	0.994
8	4.840E-2	0.999	4.841E-2	1.002
9	2.421E-2	1.000	2.421E-2	1.000

(A.4) There exists a constant $C > 0$ such that for all $w \in \widetilde{H}^2_\Gamma(\Omega)$,

$$|||\widehat{I}_k\pi_{k-1}w - w|||_k + |||P_{k-1}\pi_k w - w|||_{k-1} \le Ch_k\|w\|_{\widetilde{H}^2(\Omega)}. \tag{16}$$

We have the following spectral property of A_h.

Lemma 1 *(**Spectral property of** A_h) Let λ_h be the largest eigenvalue of $a_h(\cdot,\cdot)$, i.e., $\lambda_h = \sup_{u\in\hat{S}_h(\Omega)} \frac{a_h(u,u)}{(u,u)_h}$. Then,*

$$\lambda_h \le Ch^{-2}, \tag{17}$$

where C is a positive constant.

Proof This follows from the inverse inequality, discrete Poincare inequality in ([9, 15, 38]), and the equivalence of $|||\cdot|||_h$ and $\|\cdot\|_{1,h}$. □

To prove the assumption (A.2), we need the following Lemma.

Lemma 2 *For all $\phi \in \widehat{S}_k$ and for $T \in \mathcal{T}_k$, we have*

$$\frac{1}{C}h_k\sum_{i=1}^{3}|\phi(x_i)| \le \|\phi\|_{0,T} \le Ch_k\sum_{i=1}^{3}|\phi(x_i)|.$$

for some $C > 0$ independent of k where x_i $(i = 1, 2, 3)$ are nodes of T.

Proof We note that when $\phi \in S_k$, this equivalence is trivial. Suppose T is cut by Γ where y_1 and y_2 are intersections of Γ and edges of T_k (see Fig. 4). We first show

$$\|\phi\|_{0,T} \le Ch_k\sum_{i=1}^{3}|\phi(x_i)|. \tag{18}$$

Since $\beta^-, \beta^+ > 0$, the values of ϕ at y_1 and y_2 are intermediate values of $\phi(x_i)$. For example,

$$\min\{\phi(x_1), \phi(x_2)\} < \phi(y_1) < \max\{\phi(x_1), \phi(x_2)\}. \tag{19}$$

Since $\phi|_{T^-}$ is linear on T^- and by Taylor expansion, we have

$$\phi(x) = \phi(x_1) + \nabla\phi^- \cdot (x - x_1), \quad (x, y) \in T^-.$$

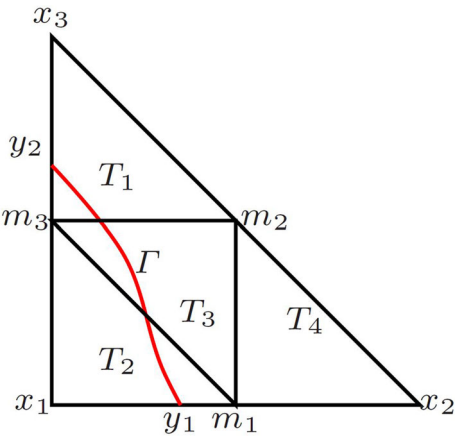

Fig. 4 Interface elements on level k and $k-1$

This implies that

$$\begin{aligned}\|\phi(x)\|^2_{T^-} \le & C|T^-|\Big((|\phi(x_1)|^2+|\phi(y_1)|^2+|\phi(y_2)|^2)+|T^-|\cdot|\nabla\phi^-|^2\Big),\\ \le & C|T^-|\Big(|\phi(x_1)|^2+|\phi(y_1)|^2+|\phi(y_2)|^2\Big), (\text{by } \phi \text{ is linear on } T^-). \quad (20)\end{aligned}$$

Similary, we have,

$$\|\phi(x)\|^2_{T^+} \le C|T^+|\left(|\phi(x_2)|^2+|\phi(x_3)|^2+|\phi(y_1)|^2+|\phi(y_2)|^2\right). \quad (21)$$

Thus, by (19), (20), and (21) and by the fact that $|T^-|, |T^+| \le h_k^2$, we have (18).

To prove the converse, we define $\gamma : \widehat{S}_k(T) \to S_k(T)$ by $\gamma\phi(x_i) = \phi(x_i)$. One of the authors of this paper proved that operator γ is bounded by some constant C (see [15]). Thus,

$$h_k \sum_{i=1}^{3} |\phi(x_i)| = h_k \sum_{i=1}^{3} |\gamma\phi(x_i)| \le C\|\gamma\phi\|_{0,T} \le C\|\phi\|_{0,T}.$$

□

Proposition 5 *There exists a constant $C > 0$ such that*

$$\|\widehat{I}_k u\|_{L^2(\Omega)} \le C\|u\|_{L^2(\Omega)}. \quad (22)$$

for $u \in \widehat{S}_{k-1}(\Omega)$.

Proof Suppose x_1, x_2, and x_3 are nodes of triangle T and m_1, m_2, and m_3 are mid points of x_i $(i = 1, 2, 3)$ (see Fig. 4). Then, by definition of $\widehat{I}_k$, we have $\phi(x_i) = \widehat{I}_k\phi(x_i)$, $i = 1, 2, 3$. Also, the values of ϕ at m_i are intermediate values of $\phi(x_i)$ and $\phi(x_{i+1})$. By Lemma 2, we have

$$\|\widehat{I}_k\phi(x)\|_{0,T} \le Ch\sum_{i=1}^{3}|\phi(x_i)| + Ch\sum_{i=1}^{3}|\phi(m_i)| \le Ch\sum_{i=1}^{3}|\phi(x_i)| \le C\|\phi(x)\|_{0,T}.$$

By summing over all elements $T \in \mathcal{T}_k$, we have the conclusion. □

We are ready to prove assumption (A.2).

Theorem 2 *There exists a constant $C^* > 0$ such that that does not depend on the location of Γ, β such that $\|\widehat{I}_k u\|_k \le C^* \|u\|_{k-1}$.*

Proof Define $w \in \tilde{H}^2(\Omega)$:

$$\begin{cases} -\nabla \cdot \beta \nabla w &= A_{k-1} u \\ w &= 0 \end{cases}$$

By definition of w and A_{k-1}, for all $\phi_{k-1} \in \widehat{S}_{k-1}$,

$$a_{k-1}(w - u, \phi_{k-1}) = (A_{k-1} u, \phi_{k-1}).$$

This implies that (see [24]),

$$\|w - u\|_0 \le h_k^2 \|w\|_{\tilde{H}^2(\Omega)}. \tag{23}$$

By (11), (17), (22), (23), and (16)

$$\begin{aligned} \|\widehat{I}_k u\|_k &\le \|\widehat{I}_k u - \widehat{I}_k \pi_{k-1} w\|_k + \|\widehat{I}_k \pi_{k-1} w - \pi_k w\|_k + \|\pi_k w - w\|_k + \|w\|_k \\ &\le h_k^{-1} \|\widehat{I}_k u - \widehat{I}_k \pi_{k-1} w\|_0 + h_k \|w\|_{\tilde{H}^2(\Omega)} + \|u\|_{k-1} \\ &\le h_k^{-1} \|u - \pi_{k-1} w\|_0 + h_k \|w\|_{\tilde{H}^2(\Omega)} + \|u\|_{k-1} \\ &\le h_k \|w\|_{\tilde{H}^2(\Omega)} + \|u\|_{k-1} \le h \|A_{k-1} u\|_0 + \|u\|_{k-1} \le C \|u\|_{k-1}. \end{aligned}$$

□

Corollary 1 *For $u \in \widehat{S}_k(\Omega)$, it holds that*

$$\|P_{k-1} u\|_{k-1} \le C^* \|u\|_k, \tag{24}$$

where a constant C^* is the same as in Theorem 2.

Finally, we show assumption (A.3) holds with $\alpha = 1/2$.

Theorem 3 *For $u \in \widehat{S}_k(\Omega)$, there exists a constant $C > 0$ such that*

$$|a_k((I - \widehat{I}_k P_{k-1}) u, u)| \le C \left(\frac{\|A_k u\|_k^2}{\lambda_k} \right)^{\frac{1}{2}} a_k(u, u)^{\frac{1}{2}}.$$

Proof By definition of $\widehat{I}_k$,

$$\begin{aligned} a_k((I - \widehat{I}_k P_{k-1}) u, u) &= a_k(u, u) - a_{k-1}(P_{k-1} u, P_{k-1} u) \\ &= a_k(u - \pi_k w, u) \\ &\quad + a_{k-1}(\pi_{k-1} w - P_{k-1} u, P_{k-1} u) \\ &\quad + a_k(\pi_k w, u) - a_{k-1}(\pi_{k-1} w, P_{k-1} u) \\ &:= \Phi_1 + \Phi_2 + \Phi_3, \end{aligned}$$

where w is a solution of

$$\begin{cases} -\nabla \cdot (\beta \nabla w) = A_k u \ \text{ in } \ \Omega, \\ [w]_\Gamma = \left[\beta \frac{\partial w}{\partial \mathbf{n}}\right]_\Gamma = 0 \\ w = 0 \quad \text{ on } \ \partial\Omega. \end{cases}$$

By the similar techniques used in Theorem 2 (see [3, 23, 25]) and by Lemma 1, Proposition 5, Corollary 1, we can bound Φ_1, Φ_2, and Φ_3. □

Finally, we verify (A.4) numerically. We let

$$w = \begin{cases} (x^2+y^2)^{\frac{3}{2}}/\beta^- & \text{in } \Omega^-, \\ (x^2+y^2)^{\frac{3}{2}}/\beta^+ + \left(\frac{1}{\beta^-} - \frac{1}{\beta^+}\right) r_0^3 & \text{in } \Omega^+. \end{cases} \tag{25}$$

on the domain $\Omega = [-1, 1]^2$, where subregion Ω^- is inside of the circle $x^2+y^2 = r_0^2$ and $\Omega^+ = \Omega - \Omega^-$. Here, $(\beta^-, \beta^+) = (1000, 1)$ and $r_0 = 0.64$. Let $\mathcal{T}_k$ be the sequence of uniform hierarchical triangulations of Ω by right triangles with size $h_k = 2^{2-k}$. Since $\|\cdot\|_{1,h_k}$ and $|||\cdot|||_k$ are equivalent norms, we report $\|\widehat{I}_k \pi_{k-1} w - w\|_{1,h_k}$ and $\|P_{k-1}\pi_k w - w\|_{1,h_k}$ in Table 1. We observe that they are of $\mathcal{O}(h)$, which coincides with (A.4). For other choices of w, we obtain similar results.

5 Numerical results

In this section, we demonstrate the performance of **LMG** and **NcMG** for IFEM discretization of (1). We tested them to various interface problems including non-convex interfaces. We report the number of iterations and convergence rates of **LMG** with one smoothing and multigrid-preconditioned conjugate gradient (MG-PCG) in Tables 2, 5, 8, and 10. We report the number of iterations and convergence rates of **NcMG** in Table 13. Here, convergence rates of the solvers are defined as usual. For example, a convergence rate of **MG** solver is measured by

$$\left(\frac{\|(I - \mathbf{MG}_J A_J)^\ell g_J\|}{\|g_J\|}\right)^{1/\ell},$$

where $\mathbf{MG} = \mathbf{LMG}$ or **NcMG**, g_J is a load vector and ℓ is number of iterations. For **LMG**, we used $\mathcal{V}(1,1)$ and for **NcMG**, we used $\mathcal{N}_7(1,1)$. In the MG-PCG, $\mathcal{V}$-cycle with one smoothing is used as a preconditioner of the CG. For the first two examples, we report the performance of **MG** for the case of $\beta^+/\beta^- = 1000$ and $1/1000$. However, for the third example, we report the performance of **MG** with various cases of β^+/β^- (see Tables 8 and 15). The number of cycles of multigrids tends to increase as the ratio of β jumps increases, i.e., $\beta^+/\beta^- = 1, 10, 100, 1000$. Still, for all the cases, the number of cycles remain bounded as level J increases.

Table 2 The number of iterations and convergence rates of $\mathcal{V}(1,1)$-cycle and MG-PCG for $\widehat{S}_J^P(\Omega)$ for Example 1

	$\mathcal{V}(1,1)$-cycle		MG-PCG	
$1/h_J$	Iter.	Ratio	Iter.	Ratio
32	38	0.693	14	0.367
64	39	0.701	15	0.394
128	27	0.598	14	0.346
256	25	0.575	12	0.313

We present condition number of $\mathcal{A}_J$ for all the examples (see Tables 4, 7, 9, 12, and 16). The condition number of $\mathcal{A}_J$ seems to grow more than $\mathcal{O}(h^{-2})$, when $\beta^+/\beta^- = 1000$ for Lagrangian-based IFEM scheme. On the other hand, the condition number grows like $\mathcal{O}(h^{-2})$ for edge average-based IFEM scheme. However, the multigrid behaviors are robust for all the problems. For the first example, we present condition numbers of $\mathbf{LMG}_J A_J$ to verify the effectiveness of the preconditioning in Table 4.

We also compare the CPU time of multigrid solvers with that of diagonally preconditioned conjugate gradient methods (D-PCG) in Tables 3, 6, 11, and 17. Both the **LMG** and **NcMG** show optimal scalability in all examples. The CPU time of multigrid solvers grows like $\mathcal{O}(N)$ while the CPU time of CG (or PCG) grows like $\mathcal{O}(N^{3/2})$. All experiments were conducted on PC with an Intel(R) Core(TM) i7-3770 CPU @ 3.40 GHz processor.

We let the domain $\Omega = [-1, 1]^2$ and we use uniform hierarchical triangulations with the mesh size $h_k = 2^{-k}h_0$ $(k = 0, 1, \ldots, J)$ where h_0 is the mesh size of the coarsest level. Figure 5 depicts the interfaces and triangulations of the domain by triangles. We use one step $(m = 1)$ of Gauss-Seidel for smoothing in all of multigrid algorithms. For all of the solvers, the stopping criteria $\|g - A_J x\|/\|g\| < 10^{-6}$ was used. We choose σ as $\sigma = \kappa\beta$ for some $\kappa > 0$.

5.1 Examples for LMG

We test three different interface problems. In each example, we show the performance of **LMG** for $\widehat{S}_J^P(\Omega)$. The performance of **LMG** for the case of $\widehat{S}_h^Q(\Omega)$ is reported for Example 1 only (see Tables 10 and 11).

Example 1 The interface is given by $\Gamma = \{(x, y) : y - 3x(x-0.3)(x-0.8) - 0.38 = 0\}$ and the coefficient is $\beta^- = 1$, $\beta^+ = 1000$. The exact solution $u(x, y)$ is

$$u(x, y) = \begin{cases} (y - 3x(x - 0.3)(x - 0.8) - 0.38)/\beta^- \text{ if } (x, y) \in \Omega^-, \\ \\ (y - 3x(x - 0.3)(x - 0.8) - 0.38)/\beta^+ \text{ if } (x, y) \in \Omega^+. \end{cases}$$

We report the performance of the $\mathcal{V}$-cycle and MG-PCG in terms of the number of iterations and convergence rates in Table 2. We observe the number of iterations are bounded independent of the levels for both the algorithms.

Table 3 shows the CPU time of the $\mathcal{V}$-cycle, MG-PCG, D-PCG, and CG. The CPU time of $\mathcal{V}$-cycle and MG-PCG outperforms that of D-PCG and CG. The multigrid solvers and MG-PCG show optimal scalability, i.e., the CPU time increases linearly

Table 3 CPU time of various solvers for $\widehat{S}_J^P(\Omega)$ for Example 1

$1/h_J$	$\mathcal{V}(1, 1)$ cycle	MG-PCG	CG	D-PCG
32	0.748	0.367	4.977	0.296
64	1.763	0.698	58.874	2.247
128	3.370	1.944	455.399	17.581
256	10.857	5.996	3628.578	132.616

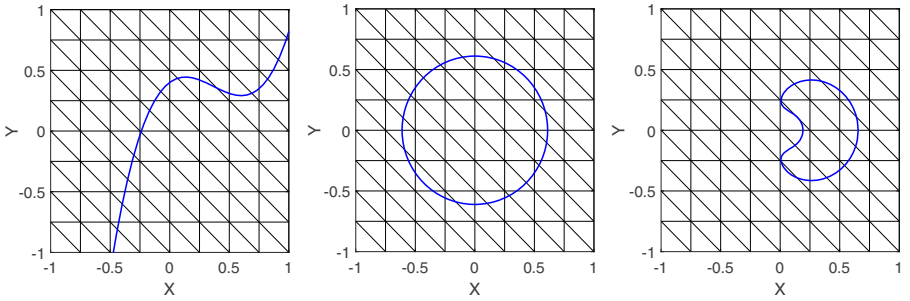

Fig. 5 Uniform meshes with a curved interface of Example 1 (left) and a circular interface of Example 2 (mid) and a heart-shaped interface of Example 3 (right)

Table 4 Condition numbers of A_J and $\mathcal{V}(1,1)A_J$ for $\widehat{S}_J^P(\Omega)$ for Example 1

$1/h_J$	$\kappa(A_J)$	$\kappa(\mathcal{V}(1,1)A_J)$
32	2.063E+6	6.529
64	9.808E+6	10.612
128	3.932E+7	6.826
256	1.720E+8	5.279

Table 5 The number of iterations and convergence rates of $\mathcal{V}$-cycle and MG-PCG for $\widehat{S}_J^P(\Omega)$ for Example 2

	$\mathcal{V}(1,1)$ cycle		MG-PCG	
$1/h_J$	Iter.	Ratio	Iter.	Ratio
32	30	0.625	14	0.336
64	44	0.723	15	0.395
128	41	0.712	17	0.443
256	33	0.658	16	0.408

Table 6 CPU time of various solvers for $\widehat{S}_J^P(\Omega)$ for Example 2

$1/h_J$	$\mathcal{V}(1,1)$ cycle	MG-PCG	CG	D-PCG
32	0.568	0.296	3.381	0.921
64	1.911	0.717	34.707	2.398
128	5.259	2.356	290.474	15.865
256	14.676	7.816	2639.282	62.665

Table 7 Condition numbers of A_J for $\widehat{S}_J^P(\Omega)$ for Example 2

$1/h_J$	$\kappa(A_J)$
32	2.957E+6
64	1.714E+7
128	8.221E+7
256	7.130E+8

as the number of unknowns increases while the CPU time of CG or D-PCG grows like $\mathcal{O}(N^{3/2})$. Among the solvers, MG-PCG gives the best performance.

Next, we report the condition numbers of $\mathbf{LMG}_J A_J$ and A_J for Example 1 in Table 4. This demonstrates that the condition numbers of $\mathbf{LMG}_J A_J$ are uniformly bounded. Thus, $\mathbf{LMG}_J$ can be used effectively as a preconditioner.

Example 2 (from [28]) The interface is given by $\Gamma = \{(x, y) : x^2 + y^2 = r_0^2\}$ where $r_0 = 0.64$ and the coefficient is $\beta^- = 1000$, $\beta^+ = 1$. The exact solution $u(x, y)$ is

$$u = \begin{cases} r^3/\beta^- & \text{in } \Omega^-, \\ r^3/\beta^+ + \left(\frac{1}{\beta^-} - \frac{1}{\beta^+}\right) r_0^3 & \text{in } \Omega^+. \end{cases}$$

We report the performance of the $\mathcal{V}$-cycle and MG-PCG in terms of the number of iterations and convergence rates in Table 5. We observe that all of the solvers have

Table 8 The number of iterations and convergence rates of $\mathcal{V}$-cycle and MG-PCG for $\widehat{S}_J^P(\Omega)$ for Example 3 with different β jumps

Case 1.	$\mathcal{V}(1, 1)$ cycle		MG-PCG	
$1/h_J$	Iter.	Ratio	Iter.	Ratio
32	9	0.193	6	0.074
64	9	0.191	6	0.074
128	9	0.187	6	0.072
256	9	0.183	6	0.070
Case 2.	$\mathcal{V}(1, 1)$ cycle		MG-PCG	
$1/h_J$	Iter.	Ratio	Iter.	Ratio
32	9	0.201	6	0.083
64	9	0.198	6	0.080
128	9	0.194	6	0.077
256	9	0.191	6	0.074
Case 3.	$\mathcal{V}(1, 1)$ cycle		MG-PCG	
$1/h_J$	Iter.	Ratio	Iter.	Ratio
32	11	0.277	8	0.151
64	10	0.233	7	0.129
128	9	0.205	7	0.113
256	9	0.195	7	0.109
Case 4.	$\mathcal{V}(1, 1)$ cycle		MG-PCG	
$1/h_J$	Iter.	Ratio	Iter.	Ratio
32	74	0.829	16	0.406
64	38	0.694	15	0.384
128	29	0.630	13	0.334
256	38	0.694	13	0.341

Case 1., Case 2., Case 3., and Case 4. correspond to $(\beta^-, \beta^+) = (1, 1)$, $(\beta^-, \beta^+) = (1, 10)$, $(\beta^-, \beta^+) = (1, 100)$, and $(\beta^-, \beta^+) = (1, 1000)$, respectively

Table 9 Condition numbers of A_J for $\widehat{S}_J^P(\Omega)$ for Example 3 with different β jumps

Case 1.	
$1/h_J$	$\kappa(A_J)$
32	1.666E+3
64	6.666E+3
128	2.656E+4
256	1.062E+5
Case 2.	
32	2.313E+3
64	9.237E+3
128	3.723E+4
256	1.482E+5
Case 3.	
32	3.189E+4
64	1.181E+5
128	6.687E+5
256	2.634E+6
Case 4.	
32	4.702E+5
64	1.847E+6
128	1.326E+7
256	1.197E+8

Case 1., Case 2., Case 3., and Case 4. correspond to $(\beta^-, \beta^+) = (1, 1)$, $(\beta^-, \beta^+) = (1, 10)$, $(\beta^-, \beta^+) = (1, 100)$, and $(\beta^-, \beta^+) = (1, 1000)$, respectively

Table 10 The number of iterations and convergence rates of $\mathcal{V}(1, 1)$ cycle and MG-PCG for $\widehat{S}_J^Q(\Omega)$ for Example 1

	$\mathcal{V}(1, 1)$ cycle		MG-PCG	
$1/h_J$	Iter.	Ratio	Iter.	Ratio
32	52	0.765	17	0.436
64	53	0.769	17	0.440
128	42	0.717	15	0.380
256	38	0.692	13	0.340

Table 11 CPU time of various solvers for $\widehat{S}_J^Q(\Omega)$ for Example 1

$1/h_J$	$\mathcal{V}(1, 1)$ cycle	MG-PCG	CG	D-PCG
32	1.233	0.406	2.929	0.249
64	2.043	0.889	27.672	2.341
128	5.722	2.246	213.112	18.247
256	17.066	6.645	1674.743	118.155

Table 12 Condition numbers of A_J for $\widehat{S}_J^Q(\Omega)$ for Example 1

$1/h_J$	$\kappa(A_J)$
32	3.614E+05
64	1.447E+06
128	5.787E+06
256	2.315E+07

optimal scalability. Table 6 compares the CPU time of the four algorithms above. Again, the multigrid-related algorithms are optimal, while CG-type algorithms are not. We report the condition number of stiffness matrix A_J in Table 7.

Example 3 The interface is given by $\Gamma = \{(x, y) : (3x^2 + 3y^2 - x)^2 - (x^2 + y^2) + 0.03 = 0\}$ and the coefficient is $\beta^- = 1, \beta^+ = 1000$. The exact solution $u(x, y)$ is

$$u = \begin{cases} x\left((3x^2 + 3y^2 - x)^2 - (x^2 + y^2) + 0.03\right)/\beta^- & \text{in}\Omega^-, \\ x\left((3x^2 + 3y^2 - x)^2 - (x^2 + y^2) + 0.03\right)/\beta^+ & \text{in}\Omega^+. \end{cases}$$

We report the performance of the $\mathcal{V}$-cycle and MG-PCG with various coefficient jumps $((\beta^-, \beta^+) = (1, 1), (1, 10), (1, 100), (1, 1000))$ in Table 8 and the condition number of stiffness matrix A_J for each case in Table 9. We note that when $\beta^- = \beta^+$, $\mathcal{V}$-cycle corresponds to the usual multigrid algorithms for P_1-conforming case. The number of required $\mathcal{V}$-cycle is 9. We observe that the number of $\mathcal{V}(1, 1)$-cycle increases as the ratio β^+/β^- increases (see Table 8). This is natural since the condition number of A_J increases as the ratio β^+/β^- increases (see Table 9). As for the fixed ratio of β^-/β^+, the numbers of $\mathcal{V}(1, 1)$-cycle are uniformly bounded as level J increases.

Finally, we report the performance of rectangular case ($\widehat{S}_J^Q(\Omega)$) in Tables 10 and 11 (for Example 1). The condition number of A_J for this case is reported in Table 12.

Table 13 The number of iterations and convergence rates of **NcMG** for Example 1; Example 2, for the spaces $\widehat{N}_J^P(\Omega)$ and $\widehat{N}_J^Q(\Omega)$

Example 1	**NcMG** ($\widehat{N}_J^P(\Omega)$)		**NcMG** ($\widehat{N}_J^Q\Omega)$)	
$1/h_J$	Iter.	Ratio	Iter.	Ratio
32	49	0.751	36	0.680
64	52	0.766	28	0.606
128	42	0.719	27	0.592
256	40	0.706	25	0.572
Example 2				
32	45	0.732	23	0.540
64	51	0.763	23	0.542
128	46	0.741	23	0.541
256	44	0.728	23	0.547

Table 14 Condition numbers of A_J for Example 1 and Example 2 for the spaces $\widehat{N}_J^P(\Omega)$ and $\widehat{N}_J^P(\Omega)$

Example 1 $1/h_J$	$\widehat{N}_J^P(\Omega)$ $\kappa(A_J)$	$\widehat{N}_J^Q(\Omega)$ $\kappa(A_J)$
32	3.242E+06	2.168E+06
64	1.302E+07	8.679E+06
128	5.209E+07	3.472E+07
256	2.084E+08	1.389E+08
Example 2		
32	5.986E+06	3.988E+06
64	2.395E+07	1.596E+07
128	9.581E+07	6.387E+07
256	3.832E+08	2.555E+08

5.2 The case of NcMG

We now test **NcMG** for the Examples in Section 5.1. The left side of Table 13 shows the performance for CR-type IFEM and the right side shows that of the RT-type IFEM for Example 1 and Example 2. We report the condition number of A_J for each

Table 15 The number of iterations and convergence rates of **NcMG** for Example 3 with different β jumps

Case 1.	**NcMG** ($\widehat{N}_J^P(\Omega)$)		**NcMG** ($\widehat{N}_J^Q\Omega)$)	
$1/h_J$	Iter.	Ratio	Iter.	Ratio
32	13	0.305	5	0.044
64	13	0.318	5	0.050
128	13	0.321	5	0.054
256	13	0.319	5	0.057
Case 2.				
32	13	0.310	5	0.044
64	13	0.319	5	0.050
128	13	0.321	5	0.054
256	13	0.319	5	0.057
Case 3.				
32	13	0.325	5	0.051
64	13	0.334	5	0.053
128	13	0.332	5	0.055
256	13	0.327	5	0.057
Case 4.				
32	39	0.701	22	0.528
64	31	0.637	20	0.498
128	27	0.595	18	0.481
256	25	0.575	18	0.463

Case 1., Case 2., Case 3., and Case 4. correspond to $(\beta^-, \beta^+) = (1, 1)$, $(\beta^-, \beta^+) = (1, 10)$, $(\beta^-, \beta^+) = (1, 100)$, and $(\beta^-, \beta^+) = (1, 1000)$, respectively

Table 16 Condition numbers of A_J for $\widehat{N}_J^P(\Omega)$ and $\widehat{N}_J^Q(\Omega)$ for Example 3 with different β jumps

Case 1. $1/h_J$	$\widehat{N}_J^P(\Omega)$ $\kappa(A_J)$	$\widehat{N}_J^Q(\Omega)$ $\kappa(A_J)$
32	7.470E+3	4.979E+03
64	2.988E+4	1.992E+04
128	1.195E+5	7.968E+04
256	4.781E+5	3.187E+05
Case 2.		
32	1.041E+4	6.926E+03
64	4.161E+4	2.771E+04
128	1.664E+5	1.109E+05
256	6.653E+5	4.434E+05
Case 3.		
32	6.204E+04	4.128E+04
64	2.476E+05	1.650E+05
128	9.900E+05	6.599E+05
256	3.959E+06	2.639E+06
Case 4.		
32	6.004E+05	3.996E+05
64	2.397E+06	1.597E+06
128	9.585E+06	6.389E+06
256	3.834E+07	2.556E+07

Case 1., Case 2., Case 3., and Case 4. correspond to $(\beta^-, \beta^+) = (1, 1)$, $(\beta^-, \beta^+) = (1, 10)$, $(\beta^-, \beta^+) = (1, 100)$, and $(\beta^-, \beta^+) = (1, 1000)$, respectively

case in Table 14. We report the performance of **NcMG** for various cases of β^+/β^- for Example 3 in Table 15. Table 16 reports the condition number of A_J for each case.

For the ratio $\beta^+/\beta^- = 1, 10, 100, 1000$, the **NcMG** for both the CR-type IFEM and RT-type IFEM requires relatively small number of iterations to reach the stopping criteria. For the fixed ratio β^+/β^-, the number of cycles of **NcMG** is uniformly bounded as J increases.

We note that **NcMG** converges when m is sufficiently large. We note that for any $m \geq 7$, the solver $\mathcal{N}_m(1, 1)$ converges uniformly for all examples. In this work, $\mathcal{N}_7(1, 1)$ was used for **NcMG**.

Table 17 CPU time of **NcMG**, CG, and D-PCG solvers for Example 3 in $\widehat{N}_J^Q(\Omega)$

$1/h_J$	**NcMG**	CG	D-PCG
32	1.562	3.659	0.748
64	2.484	31.029	6.451
128	15.209	248.811	48.060
256	57.137	1832.172	364.563

Table 17 shows the CPU time of **NcMG**, CG, and D-PCG (for Example 3) when $(\beta^-, \beta^+) = (1, 1000)$. We observe that our version of multigrid solvers is optimal, i.e., the CPU time grows like $\mathcal{O}(N)$.

6 Conclusion

In this work, we designed and tested multigrid algorithms for two kinds of IFEMs, one for Lagrangian-based IFEM (**LMG**) and the other for edge average dof-based IFEM (**NcMG**). For **NcMG**, we used the idea of projecting onto Lagrangian IFEM correction space. The numerical experiments show that **LMG** is optimal in scalability with only one smoothing. The **NcMG** multigrid solver with the inner cycle $\mathcal{V}(1, 1)$ is also optimal in scalability. The CPU time comparison with PCG or CG algorithms shows the effectiveness of our multigrid algorithms for IFEM.

References

1. Arnold, D.N., Brezzi, F., Cockburn, B., Marini, L.D.: Unified analysis of discontinuous Galerkin methods for elliptic problems. SIAM J. Numer. Anal. **39**, 1749–1779 (2002)
2. Bramble, J.H., King, J.T.: A finite element method for interface problems in domains with smooth boundaries and interfaces. Adv. Comput. Math. **6**, 109–138 (1996)
3. Bramble, J.H., Kwak, D.Y., Pasciak, J.E.: Uniform convergence of multigrid V-cycle iterations for indefinite and nonsymmetric problems. SIAM J. Numer. Anal. **31**, 1746–1763 (1994)
4. Bramble, J.H., Pasciak, J.E.: New convergence estimates for multigrid algorithms. Math. Comput. **49**, 311–329 (1987)
5. Bramble, J.H., Pasciak, J.E.: The analysis of smoothers for multigrid algorithms. Math. Comput. **58**, 467–488 (1992)
6. Bramble, J.H., Pasciak, J.E., Wang, J.P., Xu, J.: Convergence estimates for multigrid algorithms without regularity assumptions. Math. Comput. **57**, 23–45 (1991)
7. Bramble, J.H., Pasciak, J.E., Xu, J.: The analysis of multigrid algorithms with nonnested spaces or noninherited quadratic forms. Math. Comput. **56**, 1–34 (1991)
8. Brenner, S.C.: An optimal-order multigrid method for P_1, nonconforming finite elements. Math. Comput. **52**, 1–15 (1989)
9. Brenner, S.C.: Poincaré–friedrichs inequalities for piecewise H^1 functions. SIAM J. Numer. Anal. **41**, 306–324 (2003)
10. Chang, K.S., Kwak, D.Y.: Discontinuous bubble scheme for elliptic problems with jumps in the solution. Comput. Methods Appl. Mech. Eng. **200**, 494–508 (2011)
11. Chen, Z., Kwak, D.Y.: Convergence of multigrid methods for nonconforming finite elements without regularity assumptions. Comput. Appl. Math. **17**, 283–302 (1998)
12. Chen, Z.: V-cycle galerkin-multigrid methods for nonconforming methods for nonsymmetric and indefinite problems. Appl. Numer. Math. **28**, 17–35 (1998)
13. Chen, Z., Oswald, P.: Multigrid and multilevel methods for nonconforming q_1 elements. Math. Comput. Amer. Math. Soc. **67**, 667–693 (1998)
14. Chen, Z., Zou, J.: Finite element methods and their convergence for elliptic and parabolic interface problems. Numer. Math. **79**, 175–202 (1998)
15. Chou, S.H., Kwak, D.Y., Wee, K.T.: Optimal convergence analysis of an immersed interface finite element method. Adv. Comput. Math. **33**, 149–168 (2010)
16. Crouzeix, M., Raviart, P.A.: Conforming and nonconforming finite element methods for solving the stationary stokes equations i, Revue franċaise d'automatique, informatique, recherche opérationnelle. Mathématique **7**, 33–75 (1973)
17. Ewing, R.E.: The mathematics of reservoir simulation (1983)

18. Fedorenko, R.: The speed of convergence of one iterative process. USSR Comput. Math. Math. Phys. **4**, 559–564 (1964)
19. Feng, W., He, X., Lin, Y., Zhang, X.: Immersed finite element method for interface problems with algebraic multigrid solver. Commun. Comput. Phys. **15**, 1045–1067 (2014)
20. Hackbusch, W.: Multi-grid methods and applications, vol. 4 of springer series in computational mathematics (1985)
21. He, X., Lin, T., Lin, Y.: Approximation capability of a bilinear immersed finite element space. Numer. Methods Partial Differ. Equ. **24**, 1265–1300 (2008)
22. Jo, G., Kwak, D.Y.: An IMPES scheme for a two-phase flow in heterogeneous porous media using a structured grid. Comput. Methods Appl. Mech. Eng. **317**, 684–701 (2017)
23. Kwak, D.Y.: V-cycle multigrid for cell-centered finite differences. SIAM J. Sci. Comput. **21**, 552–564 (1999)
24. Kwak, D.Y., Lee, J.: A modified p_1-immersed finite element method. Int. J. Pure Appl. Math. **104**, 471–494 (2015)
25. Kwak, D.Y., Lee, J.S.: Multigrid algorithm for the cell-centered finite difference method ii: discontinuous coefficient case. Numer. Methods Partial Differ. Equ. **20**, 742–764 (2004)
26. Kwak, D.Y., Wee, K.T., Chang, K.S.: An analysis of a broken p_1-nonconforming finite element method for interface problems. SIAM J. Numer. Anal. **48**, 2117–2134 (2010)
27. Lee, C.O.: A nonconforming multigrid method using conforming subspaces. In: the Proceedings of the Sixth Copper Mountain Conference on Multigrid Methods, pp. 317–330 (1993)
28. Li, Z., Lin, T., Lin, Y., Rogers, R.C.: An immersed finite element space and its approximation capability. Numer. Methods Partial Differ. Equ. **20**, 338–367 (2004)
29. Li, Z., Lin, T., Wu, X.: New cartesian grid methods for interface problems using the finite element formulation. Numer. Math. **96**, 61–98 (2003)
30. Lin, T., Lin, Y., Rogers, R., Ryan, M.L.: A rectangular immersed finite element space for interface problems. Adv. Comput. Theory Pract. **7**, 107–114 (2001)
31. Lin, T., Lin, Y., Zhang, X.: Partially penalized immersed finite element methods for elliptic interface problems. SIAM J. Numer. Anal. **53**, 1121–1144 (2015). cited By 2
32. Lin, T., Yang, Q., Zhang, X.: A priori error estimates for some discontinuous galerkin immersed finite element methods. J. Sci. Comput. **65**, 875–894 (2015)
33. Lu, B., Zhou, Y., Holst, M., McCammon, J.: Recent progress in numerical methods for the poisson-boltzmann equation in biophysical applications. Commun. Comput. Phys. **3**, 973–1009 (2008)
34. McCormick, S.F.: Multigrid methods, vol. 3. SIAM, Bangkok (1987)
35. Nitsche, J.: ÜBer ein Variationsprinzip zur lösung von Dirichlet-Problemen bei Verwendung von teilräumen, die keinen Randbedingungen unterworfen sind. Abhandlungen aus dem mathematischen Seminar der universität Hamburg, pp. 36 (1971)
36. Rannacher, R., Turek, S.: Simple nonconforming quadrilateral stokes element. Numer. Methods Partial Differ. Equ. **8**, 97–111 (1992)
37. Roĭtberg, J.A., Šeftel', Z.: A theorem on homeomorphisms for elliptic systems and its applications. Sbornik: Math. **7**, 439–465 (1969)
38. Vohralík, M.: On the discrete poincaré–friedrichs inequalities for nonconforming approximations of the sobolev space h^1. Numer. Funct. Anal. Optim. **26**, 925–952 (2005)